A hybrid model for the charging process of the amorphous SiO_2 film in radio frequency microelectromechanical system capacitive switches*

Wang Li-Feng(王立峰)†, Huang Qing-An(黄庆安), Tang Jie-Ying(唐洁影), and Liao Xiao-Ping(廖小平)

Key Laboratory of MEMS of the Ministry of Education, Southeast University, Nanjing 210096, *China*

(Received 16 September 2010; revised manuscript received 27 October 2010)

Charging is one of the most important reliability issues in radio frequency microelectro- mechanical systems (RF MEMS) capacitive switches since it makes the actuation voltage unstable. This paper proposes a hybrid model to describe the transient dielectric charging and discharging process in the defect-rich amorphous SiO_2 RF MEMS capacitive switches and verifies experimentally. The hybrid model contains two parts according to two different charging mechanisms of the amorphous SiO_2, which are the polarisation and charge injection. The models for polarisation and for charge injection are established, respectively. Analysis and experimental results show that polarisation is always effective, while the charge injection has a threshold electric field to the amorphous SiO_2 film. Under different control voltage conditions, the hybrid model can accurately describe the experimental data.

Keywords: modeling, polarisation, charge injection, amorphous SiO_2

PACS: 77.55.–g, 77.22.–d **DOI:** 10.1088/1674-1056/20/3/037701

1. Introduction

Charge accumulation in dielectrics caused by an applied voltage is well known in scientific literature from many years ago.[1] After decades of improving the reliability of metal–oxide–semiconductor (MOS) transistors, dielectric failure rates resulting from charging problem[2,3] have been reduced to an almost imperceptible range. However, the dielectric charging behaviour of some microelectro-mechanical systems (MEMS) devices is still poorly understood and a substantial contributor to device failure. This is partly because in MEMS, the SiO_2 dielectric is often deposited under a low temperature for process compatibility. This will lead to a much higher defect concentration in the dielectric layer. In addition, the SiO_2 film in MEMS is mostly 10^2 times thicker than that in the MOS structure, even the stressed electric of the former is higher than the latter. So it is hard to tell if the MOS theory is still effective for addressing the reliability issues of MEMS.

Radio frequency (RF) MEMS capacitive switch is a sort of MEMS device. It has great potential applications for high frequency signal processing due to their excellent performance, i.e. high isolation, low insertion, low power consumption, no or negligible distortion. However, the accumulation of charges in the dielectric layer is recognized as one of the most important mechanisms that leads to stiction or fails to actuate,[4−9] and thus becomes a hot spot of study in recent years. Experimental characterization of dielectric charging in RF MEMS capacitive switch was demonstrated by the Raytheon Company for first time.[4] A simple dielectric-charging model was then set up by using the charging model of a capacitor.[5] It was reported that the dielectric charging was caused by charge injection, and the Frenkel–Poole conduction was used to roughly explain the charging mechanism.[6] An experimentally fitted analytical model[7] and a stretched exponential model[8] were two notable models for the quantitative modeling of dielectric charging. Experimental results show that dipolar polarisation can be as important as charge injection in very disordered dielectric films.[9] However, most of the existing models are not based on the dielectric charging mechanism, several models are based on just one kind of charging mechanism. It reveals that current models may be over simplified.

With this in mind, this study proposes a hybrid dielectric charging/discharging model for the RF MEMS capacitive switches which use amorphous SiO_2 film as dielectric. The paper is organized as follows:

1) To analyse the transient dielectric charging mechanisms of the amorphous SiO_2 RF MEMS ca-

*Project supported by the National Natural Science Foundation of China (Grant No. 60676043).

†Corresponding author. E-mail: wanglyfeng@hotmail.com

© 2011 Chinese Physical Society and IOP Publishing Ltd

pacitive switch, and then propose models according to these mechanisms.

2) To establish the hybrid model, and give its operation condition.

3) To explain the experimental phenomena using these mechanisms, and verify the hybrid model using the experimental data.

2. Charging mechanism and modeling of the amorphous SiO_2 film in RF MEMS capacitive switches

2.1. Foundation of the RF MEMS capacitive switch

Figure 1(a) shows the schematic diagram of an amorphous SiO_2 RF MEMS capacitive switch, the membrane bridge is formed by using the surface sacrificial layer technology.[10] When no voltage is applied, the switch is at its 'up state' and the RF signals can pass through the switch. If a DC voltage is applied, the switch membrane will be attracted down by an electrostatic force. When the applied voltage is higher than a certain pull-in voltage of the structure, the membrane will collapse and land on top of the dielectric and the RF signals will be greatly reflected from the landing position. This is called the 'down state' of the switch. Once the membrane is down, charges start to accumulate in dielectric layer under the stress of the down-state voltage. The charge accumulation is irreversible in the average switching time. Therefore, it leads to a shift of the subsequent actuation voltage. The relationship between the accumulated charge and actuation voltage shift can be given by[11]

$$\Delta V = -\frac{z}{\varepsilon} \cdot P_z, \tag{1}$$

where z is the distance from the charge layer to the bottom surface of the dielectric, P_z is the charge density at z, ε is the electric permittivity of the dielectric, as shown in Fig. 1(b), and ΔV is the actuation voltage shift caused by the accumulated charge in the dielectric.

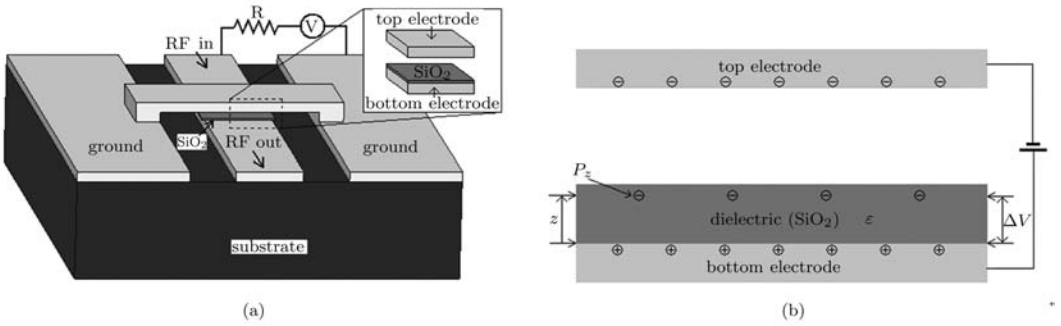


Fig. 1. An amorphous SiO_2 RF MEMS capacitive switch: (a) schematic diagram of the switch; (b) accumulated charge layer in the dielectric.

2.2. Modeling the polarisation process

One mechanism that can accumulate charges in dielectric is the polarisation. The switch response time is generally greater than 1μs. Therefore, the very fast polarisation processes, i.e., electron and atomic polarisation are neglectable. On the other hand, the dipolar polarisation and space charge polarisation processes which can last from milliseconds to minutes have to be considered. The amorphous SiO_2 used in RF MEMS capacitive switches usually possess a degree of defects, i.e., lattice imperfection or doping. Therefore, the main polarisations need to be considered here are the dipolar polarisation process caused by the reorientation of complex defects, and the space charge polarisation process caused by the translational motion of simple defects such as vacancies, ionic interstitials and defect electronic species, as shown in Fig. 2.

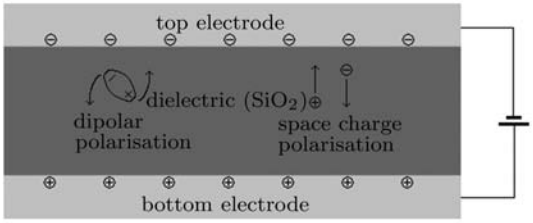


Fig. 2. Dipolar polarisation and space charge polarisation in amorphous SiO_2.

In dielectric materials, the time and temperature dependence of dipolar polarisation and depolarisation processes are determined by the competition, between the orienting action of the electric field and the randomizing action of thermal motion. However, space charge polarisation and depolarisation processes are far more complex, because several mechanisms such as the counteracting action of diffusion, recombination of carriers, the charge trapping, and the influence of local electric field can be involved simultaneously. It must be taken into account that the amorphous SiO_2 film used in the RF MEMS capacitive switch is a rather disordered system with a degree of defects. In such a system, it is more appropriate to assume that the stretched exponential law is more suitable for describing the total transient polarised charge density $P_{\rm d}$,[12]

$$P_{\rm d}(t) = P_{\rm s} \cdot \left\{1 - \exp\left[-\left(\frac{t}{\tau}\right)^{\beta}\right]\right\}, \qquad (2)$$

where t represents time, $P_{\rm s}$ is the steady state polarisation magnitude, $\beta < 1$ is the exponent, and τ is the process time scale. The polarisation time τ may achieve hundreds of seconds in amorphous SiO_2 as mentioned before. In Eq. (2) the polarisation charges are considered to be distributed on top and bottom surface of the dielectric. According to Eq. (1), only the top ones need to be considered here.

In addition, the decay of these depolarisation processes after removal of electric field is given by

$$P_{\rm d}(t) = P_{\rm p} \cdot \exp\left[-\left(\frac{t}{\tau}\right)^{\beta}\right], \qquad (3)$$

where $P_{\rm p}$ is the polarisation magnitude at the beginning of the depolarisation.

2.3. Modeling the charge injection process

Another mechanism that can accumulate charges in dielectric is the charge injection. Traps in amorphous SiO_2 are of amphoteric nature, so they can be negatively or positively charged. Once the electric field in amorphous SiO_2 reaches its threshold electric field of tunneling, the Fowler–Nordheim tunneling[13] and/or the trap assisted tunneling,[14] the conduction process starts to give rise to a spatial distribution of charges in the vicinity of the injecting contacts. This charge injection process is much similar with that of charge accumulation in the regions with discontinuous electrical parameter. So the charge injection process can be modeled through the analysis of multilayer Maxwell capacitor configuration. According to Eq. (1), the charges injected from the bottom electrode have a very small contribution to the actuation voltage shift in comparison with the top one. So a two-layer Maxwell capacitor configuration is used here to describe the charge injection of amorphous SiO_2. Figure 3(a) shows the real contact configuration of the 'down state', so the equivalent dielectric in Fig. 3(b) is made up of air and the surface of amorphous SiO_2.

Let $P_{\rm i}$ represent the injected charge density at the bottom interface of the equivalent dielectric. Following Gauss law, we can express $P_{\rm i}$ by

$$P_{\rm i}(t) = \varepsilon_{\rm e} E_{\rm e} - \varepsilon_{\rm s} E_{\rm s}, \qquad (4)$$

where $\varepsilon_{\rm e}$, $\varepsilon_{\rm s}$, and $E_{\rm e}$, $E_{\rm s}$, are the electric permittivity and the electric field of the equivalent dielectric and the amorphous SiO_2 dielectric, respectively.

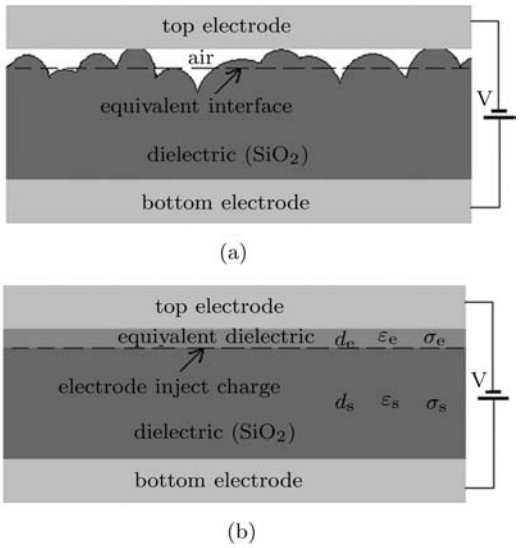


Fig. 3. Cross Sectional view of the 'down state': (a) real contact configuration; (b) two-layer Maxwell capacitor configuration.

Following the law of charge conservation at the interface, we have

$$\frac{\partial P_{\rm i}(t)}{\partial t} + (\sigma_{\rm e} E_{\rm e} - \sigma_{\rm s} E_{\rm s}) = 0, \qquad (5)$$

where $\sigma_{\rm e}$, $\sigma_{\rm s}$, are the conductivities of the two dielectrics, respectively. By using the definition of voltage potential, we have

$$d_{\rm e} E_{\rm e} + d_{\rm s} E_{\rm s} = V, \qquad (6)$$

where d_e and d_s are the thicknesses of the two dielectrics, respectively, and V is the stressed voltage between the top and bottom electrodes. Combining Eqs. (4)–(6), we obtain the transient inject charge equation by

$$\frac{\partial P_i(t)}{\partial t} + mP_i(t) = n, \tag{7}$$

where m and n are

$$m = \frac{d_s\sigma_e + d_e\sigma_s}{d_s\varepsilon_e + d_e\varepsilon_s}, \qquad n = \frac{\sigma_s\varepsilon_e - \sigma_e\varepsilon_s}{d_s\varepsilon_e + d_e\varepsilon_s}V. \tag{8}$$

The model parameters including electric permittivity and thickness can be obtained experimentally. Substituting the initial condition $P_i(t = 0) = 0$ into Eq. (7), we can derive the transient growth of charge injection process:

$$P_i(t) = \frac{n}{m} \cdot [1 - \exp(-mt)]. \tag{9}$$

When the actuation voltage is removed, the switch recovers to its 'up state'. So the equivalent dielectric becomes air, as shown in Fig. 4, its thickness $d_e >> d_s$ and its conductivity $\sigma_e << \sigma_s$. Hence, the m and n can be rewritten as

$$m \approx \frac{\sigma_s}{\varepsilon_s}, \quad n = 0, \tag{10}$$

and the transient decay process of injected charges can be obtained

$$P_i(t) = P_{i0} \cdot \exp(-mt), \tag{11}$$

where P_{i0} is the injected charges at the beginning of the decay process. Experimental results[15] show that conductivity of the SiO_2 dielectric increases much faster with the increase of the applied electric field. Therefore, conductivity of the SiO_2 dielectric in Eq. (8) will be much larger than that in Eq. (10). And $1/m$ represents the process time in Eqs. (9) and (11), the consequence is that the growth of charge injection will be much faster than its decay, leading to a time-dependent accumulation of the charges.

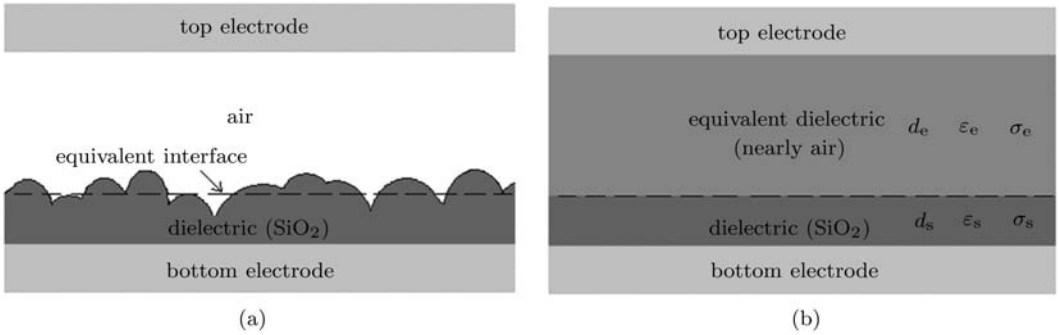


Fig. 4. Cross sectional view of the 'up state': (a) real contact configuration; (b) two-layer Maxwell capacitor configuration.

2.4. A hybrid model

Combining the two models derived above, we obtain the hybrid model for dielectric charging and discharging process in amorphous SiO_2 RF MEMS capacitive switches. Since the polarisation charge and the injection charge have the opposite polarity, the total accumulated charge P_{tot} is given by

$$P_{tot}(t) = P_d(t) - P_i(t). \tag{12}$$

However, experimental results show that polarisation is always functional for most dielectrics, while the charge injection has a threshold electric field due to the tunneling mechanism of amorphous SiO_2.[13,14,16] Hence, when the applied electric field in amorphous SiO_2 is lower than the tunneling threshold electric field, P_{tot} is only determined by polarisation. Using Eqs. (1)–(3) and (12), and assuming that the polarisation charges are on top surface of the dielectric, we find that the transient charging and discharging actuation voltage shifts of the switch are

$$\Delta V(t) = -\frac{d_s}{\varepsilon_s} \cdot P_s \cdot \left\{1 - \exp\left[-\left(\frac{t}{\tau}\right)^{\beta}\right]\right\}, \tag{13}$$

$$\Delta V(t) = -\frac{d_s}{\varepsilon_s} \cdot P_p \cdot \exp\left[-\left(\frac{t}{\tau}\right)^{\beta}\right]. \tag{14}$$

Moreover, when the applied electric field in amorphous SiO_2 is higher than the tunneling threshold electric field, P_{tot} is then determined by polarisation and charge injection both. Combining Eqs. (1)–(3), (9), (11) and (12), we find that the transient charging and discharging actuation voltage shifts of the switch are

$$\Delta V(t) = -\frac{d_{\rm s}}{\varepsilon_{\rm s}} \cdot \left(P_{\rm s} \cdot \left\{ 1 - \exp\left[-\left(\frac{t}{\tau} \right)^{\beta} \right] \right\} - \frac{n}{m} \cdot [1 - \exp(-mt)] \right), \tag{15}$$

$$\Delta V(t) = -\frac{d_{\rm s}}{\varepsilon_{\rm s}} \cdot \left(P_{\rm p} \cdot \exp\left[-\left(\frac{t}{\tau} \right)^{\beta} \right] - P_{\rm i0} \cdot \exp(-mt) \right). \tag{16}$$

3. Experimental verification

The hybrid model presents a reasonable and comprehensive explanation for the actuation voltage shift phenomena[17] which are unexplainable with the former models. The RF switch is fabricated on a glass substrate, the dielectric is the sputtered SiO_2 with a thickness of 0.25 μm, the top electrode is 0.3 μm Al membrane, the bottom electrode Cr/Au serves as the signal line of the coplanar waveguide, and the air gap between top electrode and the dielectric is 2.5 μm. The average actuation voltage of the switches is 26 V. The actuation voltage shifts for positive and negative voltage stresses are shown in Figs. 5 and 6, while the positive voltage stress means that the bottom electrode is the positive polarity.

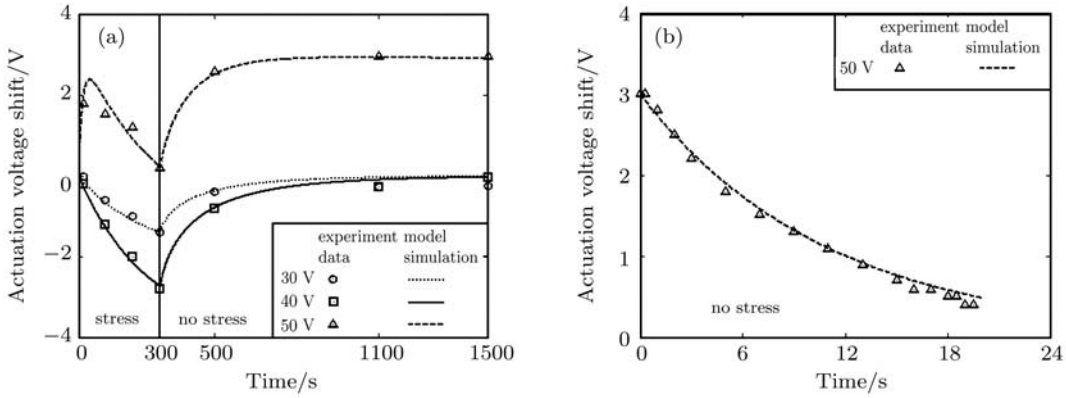


Fig. 5. Comparison of model simulation between experimental data under positive voltage stresses: (a) short time comparison during and after 30 V, 40 V, and 50 V stresses; (b) long time comparison after 50 V stress.

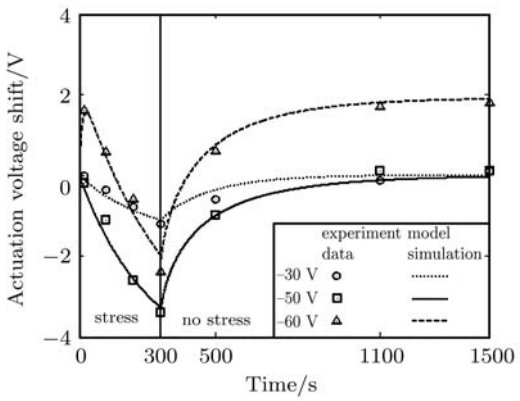


Fig. 6. Short time comparison of model simulation between experimental data during and after –30 V, –50 V, and –60 V negative voltage stresses.

In Fig. 5(a), the actuation voltage shifts under 30 V and 40 V positive voltage stresses are only determined by the polarisation mechanism. So the shifts of the actuation voltage during and after the stress process can simply be described by the polarisation mechanism. During the stress process, the polarity of the polarisation charges on top of the dielectric is opposite to that of the charges in the top electrode, so the actuation voltages keep decreasing. After the stress process, the polarisation charges disappears, and the voltage shifts return to zero.

When the switch is stressed by 50 V positive voltage, there is an abrupt change at the starting end of the curve. It clearly corresponds to a tunneling behaviour of the charge injection mechanism, with the positive tunneling threshold electric field estimated to be 2.0×10^6 V/cm. Under the positive voltage stress, electrons are tunneled into dielectric. They repel the negative polarity of top electrode and increase the actuation voltage. However, the polarisation process is still in effect. It makes the curve shift toward the opposite direction. Once the 50 V positive stress is removed, depolarisation and injection discharging are started simultaneously. The depolarisation process is quite similar to those in the 30 V and 40 V cases, so that their curve profiles are almost the same in this region. However, the duration of the injection discharging is much longer than the depolarisation, be-

cause the conductivity of the unstressed amorphous SiO_2 film is very small. It is clearly seen that the injected charges do not completely disappear even after 18 hours of discharging, as shown in Fig. 5(b).

Figure 6 shows the actuation voltage shifts under negative voltage stresses. It is seen that the curves are very similar to those of the positive voltage cases. The charge injection does not happen until the negative voltage stress reaches –60 V, so the negative tunneling threshold is estimated to be 2.4×10^6 V/cm. The different tunneling thresholds imply that the electron injection under positive voltages is easier than the hole injection under negative voltages.

The comparison of the hybrid model results with the experimental data under different voltages are shown in Figs. 5 and 6, respectively. The model parameters are fitted numerically using Matlab software, as listed in Table 1. It is clear that the hybrid model successfully predicts the complex profile of the actuation voltage shift under small and large voltage stresses.

Table 1. Extracted model parameters.

voltage stress states		polarisation				charge injection		
		τ/s	β	$P_s/(\times10^{-4}$ C/m$^2)$	$P_p/(\times10^{-4}$C/m$^2)$	$(1/m)$/s	$(n/m)/(\times10^{-4}$ C/m$^2)$	$P_{io}/(\times10^{-4}$ C/m$^2)$
30 V	Yes	250	1	–2.83				
	No	130	0.7		–1.98			
40 V	Yes	250	1	–5.50				
	No	140	0.7		–3.77			
50 V	Yes	300	1	–6.66		15	4.53	
	No	100	0.85		–3.97	39600		4.25
–30 V	Yes	250	1	2.27				
	No	180	0.95		1.56			
–50 V	Yes	250	1	6.66				
	No	150	0.7		4.82			
–60 V	Yes	350	1	10.6		11	–3.26	
	No	150	0.7		5.92			

As we have mentioned above, the amorphous SiO_2 is quite different from that in conventional MOS structure since it is thicker, defect-richer and subjected to higher electric stresses. So it is helpful to make a brief insight into the conductivity of the material. Equations (8) and (10) and Table 1 are used to calculate the results. In addition, some other parameters still need to be determined. The down-state thickness of the equivalent dielectric takes the value of 0.05 μm, which is the average roughness of metal–dielectric interface. The expression of the induced polarisation in a dielectric sphere in the presence of an external electric field[18] is used to calculate the electric permittivity of the equivalent dielectric ε_e in Fig. 3(b),

$$\varepsilon_e = \frac{3\varepsilon_s}{\varepsilon_s + 2\varepsilon_0} \cdot \varepsilon_0. \tag{17}$$

Using the above parameters, we obtain the conductivities of amorphous SiO_2 under different voltage stresses and list them in Table 2.

The results show that the conductivities of amorphous SiO_2 under voltage stresses beyond the tunneling threshold voltage are several orders of magnitude larger than that under no voltage stress. They dramatically increase with the applied voltages as expected.

Table 2. Conductivity of amorphous SiO_2.

voltage stress state	0 V	50 V	–60 V
σ_s/(S/m)	8.9×10^{-16}	2.5×10^{-12}	3.3×10^{-12}

4. Conclusion

In summary, we propose that the charging and discharging processes in the amorphous SiO_2 in RF MEMS capacitive switch are determined by two mechanisms, i.e. the polarisation mechanism including the dipolar polarisation and the space charge polarisation, and the charge injection mechanism. The hybrid model resulted from the stretched exponential law and the two-layer Maxwell capacitor configuration fits well with the experimental data of charg-

ing and discharging. It is clearly seen that the decay of the injected charges is much longer than the decay of the polarised charges, so the charge injection is highly responsible for the long-term reliability of the RF MEMS switch under high control voltages. Hence, we strongly recommend that the applied voltage beyond the threshold voltage of tunneling should be avoided. The experiment-extracted conductivities of the amorphous SiO_2 under different voltage stresses are also obtained. The hybrid model established here is helpful for better understanding of the charging mechanism and the reliability improvement of the amorphous SiO_2 RF MEMS capacitive switches in the future.

Acknowledgements

The authors wish to acknowledge the assistance and support of the MEMS laboratory of Southeast University.

References

[1] Hopkinson J and Wilson E 1897 *Philos. Trans. R. Soc. London* **189** 109
[2] Nicollian E R and Brews J R 1982 *MOS (Metal Oxide Semiconductors) Physics and Technology* (New York: Wiley) p492
[3] Ren H X and Hao Y 2001 *Chin. Phys.* **10** 189
[4] Goldsmith C, Ehmke J, Malczewski A, Pillans B, Eshelman S, Yao Z, Brank J and Eberly M 2001 *IEEE MTT-S Int. Microwave Symp. Dig.* **1** 227
[5] Yuan X, Hwang J C M, Forehand D and Goldsmith C L 2005 *IEEE MTT-S Int. Microwave Symp. Dig.* **1** 753
[6] Mellé S, De Conto D, Mazenq L, Dubuc D, Grenier K, Bary L, Vendier O, Muraro J L, Cazaux J L and Plana R 2005 *IEEE MTT-S Int. Microwave Symp. Dig.* **1** 757
[7] Spengen W M, Peurs R, Mertens R and Wolf I D 2004 *J. Micromech. Microeng.* **14** 514
[8] Papaionnou G J, Exarchos M, Theonas V, Wang G and Papapolymerou 2005 *J. IEEE MTT-S Int. Microwave Symp. Dig.* **1** 761
[9] Papaioannou G, Papapolymerou J, Pons P and Plana R 2007 *Appl. Phys. Lett.* **90** 233507-1
[10] Shi S L, Chen D P, Jing Y P, Ou Y, Ye T C and Xu Q X 2010 *Chin. Phys.* B **19** 076802
[11] Wibbeler J, Pfeifer G and Hietschold M 1998 *Sens. Actuators* A **71** 74
[12] Exarchos M, Theonas V, Pons P, Papaioannou G J, Melle S, Dubuc D, Cocetti F and Plana R 2005 *Microelectron. Reliab.* **45** 1782
[13] Lenzlinger M and Snow E H 1969 *J. Appl. Phys.* **40** 278
[14] Chou A I, Lai K, Kumar K, Chowdhury P and Lee J C 1997 *Appl. Phys. Lett.* **70** 3407
[15] Riccò B, Gozzi G and Lanzoni M 1998 *IEEE Trans. Electron Devices* **45** 1554
[16] Naito M, and Beasley M R 1987 *Phys. Rev.* B **35** 2548
[17] Peng Z, Yuan X, Hwang J C M, Forehand D and Goldsmith C L 2006 *Proc. of Asia Pacific Microwave Conf.* **1**
[18] Jackson J D 1999 *Classical Electrodynamics* (New York: Wiley) p158